LBNL-59511
February 2006

Direct Space Charge Effects on the ILC Damping Rings: Task Force Report*

M. Venturini
Lawrence Berkeley National Laboratory,
Berkeley, CA, 94720 (USA),
K. Oide
KEK, Oho, Tsukuba, Ibaraki 305-0801 (Japan).

Abstract

In 2005 a global effort was initiated to conduct studies for a baseline recommendation for the various components of the International Linear Collider (ILC). Work for the damping rings was subdivided in a number of tasks. This Report contains the contribution to this effort by the Authors as Coordinators of the Task Force on space charge. (A slightly reduced version of this document can also be found as part of the 'Configuration Studies and Recommendations for the ILC Damping Rings', Edts. A. Wolski, *et al.*, LBNL-Report-59449.) The studies documented in this Report were carried out for several of the reference lattices considered for the baseline recommendation. Space charge effects were found to be quite noticeable in the lattices with the longest circumference. Although it does not appear that they could prevent operation of any machine having such lattices they do favor a choice of a ring design with shorter ($\leq$ 6km) circumference at 5 GeV.

*Work supported by Department of Energy contract DE-AC02-05CH11231

1 Introduction

Typically, space charge effects are irrelevant in lepton storage rings but they have the potential to impact the performance of the ILC (International Linear Collider) damping rings's (DR) because of the unusual combination of long circumference, small emittance, and the energy range where the damping rings are expected to operate. A signature of the importance of space charge is the linear vertical tuneshift, which could be above 0.20 for the longest proposed lattices.

While space charge is not expected to be of any consequence on injection efficiency or dynamic aperture, as it becomes relevant to the beam dynamics only toward the end of the damping cycle, it could cause an unacceptable degradation of the 20 nm (normalized) vertical emittance desired at extraction.

Because the vertical is so much smaller than the horizontal emittance, vertical motion is particularly vulnerable to the presence of any mechanism that may favor coupling with the other degrees of freedom. There are two basic ways by which space charge could have an adverse effect: by enlarging the width of already exiting lattice resonances through tune depression and by driving new resonances. In the course of this study we found evidence for both of these mechanisms.

Space charge could also affect the achievement of the target vertical equilibrium emittances in the presence of radiation by affecting the horizontal/vertical linear coupling in a linearly coupled lattice. We found indication that this effect could be noticeable but we have not yet performed a systematic investigation.

We carried out our study by numerical tracking using the codes SAD [1] and MaryLie/Impact (MLI) [2]. The modelling in both codes is based on a weak-strong approximation and the space charge force is calculated as if produced by a 6D (in phase space) gaussian bunch matched to the linear lattice. This is a reasonable approximation for the bunch distribution in damping rings close to the end of the damping cycle. We tracked particles initially distributed according to the bunch density at equilibrium including the effect of lattice nonlinearities and with space charge force applied in the kick approximation. Radiation effects were not included.

Because of the nature of the weak-strong approximation any detected emittance growth is likely to be overestimated in comparison with a more self-consistent calculation. However, the main objective here was not to quantify the emittance degradation exactly, which would require more advanced modelling, but establish whether there would exist conditions for no growth at all that could be indicated for safe operation of the machines.

The results obtained using SAD and MLI are reported in two separate sections, containing further details on the specifics about the simulations. In presenting our results we placed emphasis on exploration of the tune space and determination of offensive resonances. Some calculations were repeated with both codes for reciprocal validation. The agreement in the outcome between the two codes was generally good.

Overall we surveyed most of the proposed lattices including some of their variants (for example, in addition to the original 'C-shaped'[†] TESLA DR lattice we also considered an 'S-

[†]The 'C' is in reference is to the lattice layout.

shaped' design with better symmetry properties; for the MCH lattice we took in consideration multiple choices of RF voltage; and for both the MCH and TESLA DR lattices we also studied the option of using 'coupling bumps'). In our investigation we did not include the smallest lattices PPA, OTW (on the assumption that space charge should have negligible effects), and the DAS lattice (on the basis of its similarities with the other dogbone lattices)[3].

2 Space charge study using MLI

2.1 Basic features of the model

MaryLie/Impact is a hybrid combining MaryLie routines for lattice design, map calculation, and tracking and Impact features for space charge calculations, which allow for fully self-consistent beam dynamics simulations. However, the existing capabilities of MaryLie/Impact are not well suited for the fast evaluation of space-charge effects needed for large machines like the ILC damping rings and, we believe, not necessary. Instead, we developed the additional routines needed for modelling space charge in the weak-strong approximation. In this approximation the space charge force is calculated as if produced by an unperturbed 6D gaussian bunch matched to the linear lattice.

The lattice elements (including the drifts) are split into a number of slices and space-charge forces are applied in the kick approximation in their middle. Particle propagation between space charge-kicks is carried out using symplectic tracking. In our study we did not include radiation effects and limited our simulations of the dynamics to the end of the damping cycle where the beam sizes are the smallest and space charge forces the largest.

A further simplification comes from exploitation of the the ultra relativistic nature of the particle motion that causes the beam-generated electric and magnetic fields to appear mostly transverse in the lab frame, prompting us to neglect longitudinal space-charge effects altogether. Effectively, this amounts to assuming that a test particle at location z along the longitudinal axis with respect to the bunch center is affected only by source particles with the same longitudinal coordinate. In other words, we can calculate the transverse space charge forces at z as if the bunch was infinitely long with uniform transverse density equal to the 2D gaussian transverse density of the actual bunch at z. A major benefit of these assumptions is the existence of a closed-form solution for the resulting 2D Poisson equation if in addition we assume an open boundary condition - this last assumption is justified by the small beam transverse size compared to the vacuum chamber aperture [5].

In our model we allow for the ellipses representing isodensities of the transverse charge distribution to be tilted (see Fig. 1) with respect to the accelerator x-y plane transverse to the beam propagation. Indicate with ξ and η the coordinates along the principal axes of those isodensity ellipses and with π_ξ and π_η the canonically conjugated momenta for a particle relative to this frame. Upon introducing the complex number notation $\boldsymbol{\pi}(s) = \pi_\xi(s) + i\pi_\eta(s)$ the evolution of $\boldsymbol{\pi}$ for a charged particle in the in the sole presence of space charge can be written as

$$\frac{d\boldsymbol{\pi}}{ds} = \boldsymbol{F}, \tag{1}$$

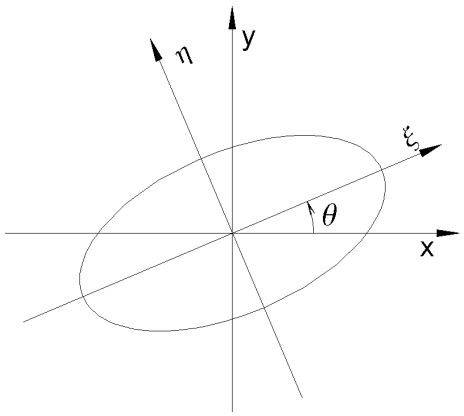

Figure 1: Beam transverse isodensity and coördinate frames.

with

$$\boldsymbol{F} = 2\sqrt{\pi}\frac{r_e}{\gamma^3}\frac{n(z)}{S}\left[w\left(\frac{\xi+i\eta}{S}\right)e^{-\frac{\xi^2}{2\sigma_\xi^2}-\frac{\eta^2}{2\sigma_\eta^2}} + w\left(\frac{\xi\frac{\sigma_\eta}{\sigma_\xi}+i\eta\frac{\sigma_\xi}{\sigma_\eta}}{S}\right)\right] \tag{2}$$

where $S = \sqrt{2(\sigma_\xi^2 - \sigma_\eta^2)}$, σ_ξ and σ_η are the rms bunch sizes in the ξ and η directions, r_e the classical radius of the electron, γ the relativistic factor, $w(z)$ the error function of complex argument, $n(z)$ the longitudinal bunch density. For a gaussian bunch $n(z) = \exp(-z^2/2\sigma_z^2)/\sqrt{2\pi}\sigma_z$.

Not surprisingly Eq. (2) is almost identical to the expression widely used in weak-strong beam-beam models for lepton colliders [4] as the set of assumptions made in the two cases are very similar (purely transverse fields; gaussian bunches). Indeed, Eq. (2) can be recovered from the expression of the beam-beam force simply by multiplying by $1/2\gamma^2$. The factor $1/\gamma^2$ accounts for the nearly cancellation of magnetic and electric forces experienced by a test particle comoving with the rest of the beam. In contrast, the electric and magnetic forces as experienced by a test particle moving against a colliding beam, add up - with the two forces being almost equal in magnitude in the ultrarelativistic limit (factor 1/2).

For numerical evaluation of Eq. (2) we used a Padé approximant representation of the error function of complex argument $w(z)$ implemented in a routine based on work by R. Talman [6]. We carried out numerical tests to check the accuracy of this approximation against evaluation done using *Mathematica* [7] built-in functions - which are believed to be accurate through machine precision. We found relative deviations of order 10^{-6} or better at points in the beam core and 10^{-3} at points outside the core, where the strength of the kick, however, is considerable smaller.

Having determined the space-charge force in the ξ-η plane (generally tilted by an angle θ) it is just a matter of carrying out a rotation to recover the equations of motions $dp_x/ds = f_x$ and $dp_y/ds = f_y$ in the x-y plane. We have $(f_x(x,y), f_y(x,y)) = \boldsymbol{R}(\theta)(\mathrm{Re}\,\boldsymbol{F}(\xi,\eta), \mathrm{Im}\,\boldsymbol{F}(\xi,\eta))$

with $\xi = x\cos\theta + y\sin\theta$ and $\eta = -x\sin\theta + y\cos\theta$, and

$$\boldsymbol{R}(\theta) = \begin{pmatrix} \cos\theta & -\sin\theta \\ \sin\theta & \cos\theta \end{pmatrix}. \tag{3}$$

In the kick approximation the space charge force is applied impulsively leaving the transverse position of a particle unchanged while inducing the momentum variations $\Delta p_x = L f_x$ and $\Delta p_y = \Delta L f_y$ where ΔL is the length of the lattice element slice originating the space-charge kick (we recall that we apply the kick in the middle of each slice and long elements may be cut into multiple slices). At each location where the space-charge kick is applied we need knowledge of the relative position z of a particle with respect to the bunch center, the transverse rms bunch sizes σ_ξ, σ_η, the longitudinal rms size σ_z, and the tilt angle θ.

Finding σ_ξ, σ_η, and σ_z is a two-step process. We start from the 6×6 sigma matrix $\boldsymbol{\Sigma}_{ij} = \langle z_i z_j \rangle$ evaluated at s, the last point of application of the space-charge kick, as calculated in the accelerator layout variables $z_i = (x, p_x, y, p_y, z, \delta)$. By denoting with $\boldsymbol{M}_{s\to s'}$ the transfer matrix between s and the present location s', the sigma-matrix $\boldsymbol{\Sigma}'$ at s' is given by the equation

$$\boldsymbol{\Sigma}' = \boldsymbol{M}_{s\to s'} \boldsymbol{\Sigma} \boldsymbol{M}^T_{s\to s'}. \tag{4}$$

We then extract from $\boldsymbol{\Sigma}'$ the reduced 3×3 matrix $\boldsymbol{\Sigma}'_{\rm red}$ consisting of the second moments of the charge density, i.e.

$$\boldsymbol{\Sigma}'_{\rm red} = \begin{pmatrix} \langle x^2\rangle & \langle xy\rangle & \langle xz\rangle \\ \langle yx\rangle & \langle y^2\rangle & \langle yz\rangle \\ \langle xz\rangle & \langle zy\rangle & \langle z^2\rangle \end{pmatrix}. \tag{5}$$

After diagonalization, σ_z^2 σ_ξ^2, and σ_η^2 are identified as the first, second and third largest eigenvalues of $\boldsymbol{\Sigma}'_{\rm red}$, whereas the tilt angle θ is extracted from the corresponding eigenvectors.

In this treatment we make the assumption that the lattice functions do not vary significantly over the bunch length and can be taken as equal to the value of the lattice functions in the center of the bunch. Because the design bunch length is small (between 6 and 9 mm), this approximation seems justified.

2.2 Matching of Initial Distribution

Because we are interested in studying beams close to equilibrium we require that the Σ-matrix used in space-charge force evaluation be matched to the linear lattice. The matched Σ-matrix can be found in the following way. Consider a circular (or more generally periodic) lattice, and let $\boldsymbol{M}$ be the one-turn transfer matrix from and back to a specific point in the lattice. A bunch distribution is said to be linearly matched if the sigma-matrix is invariant by propagation under $\boldsymbol{M}$. That is

$$\boldsymbol{\Sigma} = \boldsymbol{M}\boldsymbol{\Sigma}\boldsymbol{M}^T. \tag{6}$$

The solution to this equation is found by first reducing the matrix $\boldsymbol{M}$ to normal form. If $\boldsymbol{M}$ normalizable (this is necessarily true for functioning machines) we can find a (generally

not unique) transformation matrix $\boldsymbol{A}$ such that $\boldsymbol{M} = \boldsymbol{A}\boldsymbol{N}\boldsymbol{A}^{-1}$ where $\boldsymbol{N}$ (the normal form) is block diagonal with the three diagonal blocks consisting of 2×2 rotations.

Next, let $\mathbf{1}$ and $\mathbf{0}$ be the 2×2 identity and null matrix, and introduce the 6×6 matrices

$$\boldsymbol{I}_I = \begin{pmatrix} \mathbf{1} & \mathbf{0} & \mathbf{0} \\ \mathbf{0} & \mathbf{0} & \mathbf{0} \\ \mathbf{0} & \mathbf{0} & \mathbf{0} \end{pmatrix}, \qquad \boldsymbol{I}_{II} = \begin{pmatrix} \mathbf{0} & \mathbf{0} & \mathbf{0} \\ \mathbf{0} & \mathbf{1} & \mathbf{0} \\ \mathbf{0} & \mathbf{0} & \mathbf{0} \end{pmatrix}, \qquad \boldsymbol{I}_{III} = \begin{pmatrix} \mathbf{0} & \mathbf{0} & \mathbf{0} \\ \mathbf{0} & \mathbf{0} & \mathbf{0} \\ \mathbf{0} & \mathbf{0} & \mathbf{1} \end{pmatrix}. \tag{7}$$

Then the desired $\Sigma-$matrix for a matched beam is

$$\boldsymbol{\Sigma} = \boldsymbol{A}(\varepsilon_I \boldsymbol{I}_I + \varepsilon_{II} \boldsymbol{I}_{II} + \varepsilon_{III} \boldsymbol{I}_{III})\boldsymbol{A}^T, \tag{8}$$

where ε_I, ε_{II}, and ε_{III} are the three rms eigen-emittances. Eq. (8) can be verified to be solution of (6) by direct substitution and using the fact that $\boldsymbol{N}$ and $\boldsymbol{I}_i$ commute. In the absence of coupling the rms eigen-emittances ε_I, ε_{II}, and ε_{III}, coincide with the familiar horizontal, vertical, and longitudial rms emittances.

At any other points $s' \neq s$ along the lattice, the $\Sigma-$matrix can be determined either by repeating the above procedure and using the one-turn map from and to point s', or more efficiently by propagating the sigma matrix from s' to s using Eq. (4).

Knowledge of the transformation matrix $\boldsymbol{A}$ is also used to generate the initial particle gaussian distribution to be tracked. One starts with assigning a 6D gaussian particle distribution in the normalized variables $\boldsymbol{Z} = \boldsymbol{A}\boldsymbol{z}$ - this is easily done as all three degrees of freedom are orthogonal - and then the transformation $\boldsymbol{A}^{-1}$ is applied.

At least formally this procedure can also be generalized to matching to a nonlinear lattice. In this case instead of the transfer matrix one is presented with a (symplectic) nonlinear transfer map $\mathcal{M} = \mathcal{A}^{-1}\mathcal{N}\mathcal{A}$, its normal $\mathcal{N}$ and the nonlinear transformation $\mathcal{A}$. Applying the transformation $\mathcal{A}$ to the particle distribution in the normalized variables yields a distribution that is, in principle, invariant under the action of the full map $\mathcal{M}$. In practice, if the nonlinearities are significant this invariance will be only approximate. There are two reasons for this. The transformation $\mathcal{A}$ is typically constructed as a power series in the dynamical variables and unless the underlying system is integrable its convergence is not guaranteed (and this is the typical case encountered in accelerator physics). Even if the series did converge in any practical calculation one would have to introduce truncations. In any case, even retaining few terms in the series for $\mathcal{A}$ may be sufficient to preserve some degree of invariance of the eigen-emittances (which are exact invariant only in linear approximation). In our tracking we almost always used an initial particle distribution matched through third order. By doing so we found that, indeed, the eigen-emittances of the tracked distribution (without space charge) exhibited generally better invariance.

2.3 Linear Space-Charge Tuneshift

Linear tuneshift in an important figure of merit to rank the impact space charge on the lattice. The first-order space-charge tuneshift experienced by particles performing small

Table 1: Relevant Parameters for selected lattice designs ($N = 2 \times 10^{10}$, $\varepsilon_y = 2$pm).

Lattice‡	C (Km)	σ_z (mm)	ε_x (nm)	ε_z (μm)	ν_x	ν_y	ν_s	$\Delta\nu_x$	$\Delta\nu_y$
TESLA DR	17.0	6.0	0.50	8.0	76.31	41.18	0.075	-0.019	-0.313
MCH/65MV	15.9	7.8	0.68	9.0	75.78	76.41	0.188	-0.009	-0.176
MCH/65MV w/b	15.9	7.8	0.68	9.0	75.78	76.41	0.188	-0.009	-0.038
MCH/115MV	15.9	6.9	0.68	9.0	75.78	76.41	0.251	-0.010	-0.199
MCH/115MV w/b	15.9	6.9	0.68	9.0	75.78	76.41	0.251	-0.011	-0.041
OCS	6.1	5.8	0.56	7.8	50.84	40.80	0.036	-0.002	-0.083
PPA	2.8	6.0	0.43	7.6	47.81	47.68	0.027	-0.001	-0.021

oscillations around the beam centroid in a uncoupled lattice and for a gaussian bunch are

$$\Delta\nu_x = -\frac{1}{4\pi}\frac{2r_e}{\beta^2\gamma^3}\int_0^C \frac{\lambda\beta_x}{\sigma_x(\sigma_x+\sigma_y)}ds \tag{9}$$

$$\Delta\nu_y = -\frac{1}{4\pi}\frac{2r_e}{\beta^2\gamma^3}\int_0^C \frac{\lambda\beta_y}{\sigma_y(\sigma_x+\sigma_y)}ds, \tag{10}$$

where β_x, β_y are the lattice functions, σ_x, σ_y the horizontal and vertical rms beam sizes. In the absence of linear coupling $\sigma_x^2 = \varepsilon_x\beta_x + \langle\delta^2\rangle D^2$, with D being the dispersion. The expression for the longitudinal peak density, $\lambda(s) = N/\sqrt{2\pi}\sigma_z(s)$, is kept under the integral because in some cases (notably MCH) the rms bunch bunch length can vary along the lattice.

The case where the lattice is linearly coupled is relevant for the dogbone lattices with coupling bumps, which are designed to tame the effect of space charge in the vertical plane by enlarging the vertical beam in the long straight sections. A first order-calculation for the tuneshifts in this case yields [11]

$$\delta\nu_I = -\frac{1}{4\pi}\int_0^C ds[F_{11}A_{11}^2 + 2F_{12}A_{11}A_{31} + F_{22}(A_{31}^2 + A_{32}^2)], \tag{11}$$

$$\delta\nu_{II} = -\frac{1}{4\pi}\int_0^C ds[F_{11}(A_{13}^2 + A_{14}^2) + 2F_{12}A_{13}A_{33} + F_{22}A_{33}^2], \tag{12}$$

where F_{ij} are the entries of the 2×2 matrix

$$\boldsymbol{F} = \frac{2\lambda r_e}{\beta^2\gamma^3}\begin{pmatrix} \frac{\cos^2\theta}{\sigma_\xi(\sigma_\xi+\sigma_\eta)} + \frac{\sin^2\theta}{\sigma_\eta(\sigma_\xi+\sigma_\eta)} & \frac{\cos\theta\sin\theta}{\sigma_\xi(\sigma_\xi+\sigma_\eta)} - \frac{\cos\theta\sin\theta}{\sigma_\eta(\sigma_\xi+\sigma_\eta)} \\ \frac{\cos\theta\sin\theta}{\sigma_\xi(\sigma_\xi+\sigma_\eta)} - \frac{\cos\theta\sin\theta}{\sigma_\eta(\sigma_\xi+\sigma_\eta)} & \frac{\sin^2\theta}{\sigma_\xi(\sigma_\xi+\sigma_\eta)} + \frac{\cos^2\theta}{\sigma_\eta(\sigma_\xi+\sigma_\eta)} \end{pmatrix}. \tag{13}$$

‡The TESLA DR lattice is the original design contained in the TESLA TDR [8]; 'w/b' indicates that the coupling bumps are turned on; the qualification 65MV and 115MV for the MCH lattice refers to the total RF voltage. The MAD deck as posted on the ILC DR web site specifies a 65MV voltage. The corresponding rms bunch length, however, is 10% smaller than the 9 mm design value.

If the rms bunch length σ_z is not unform along the lattice (as in MCH) the number specified in the Table refers to the largest value.

For tracking we used the longitudinal emittances as reported, which are the same as the natural emittances (except for the MCH/65MV lattice, which has natural emittance $\varepsilon_z = 11$ μm). The tuneshifts reported for the OCS lattice are relative to $\varepsilon_y = 1$ pm (not 2 pm).

In (11) and (12), A_{ij} are the $s-$dependent entries of the matrix $\boldsymbol{A}_s$ (in the gauge $\boldsymbol{A}_{12} = \boldsymbol{A}_{34} = 0$) normalizing the one-turn unperturbed transfer matrix $\boldsymbol{M}$ at s.

Table 1 summarizes the tuneshift values as calculated from linear theory for selected lattices. Those numbers were obtained for a $\varepsilon_y = 2$ pm vertical eigen-emittance and the lattice natural horizontal emittance. These values are somewhat smaller than the 0.8 nm horizontal emittance meeting specifications and result in correspondingly larger tuneshift estimates.

To make comparison with tuneshift evaluations presented elsewhere we should point out that the calculation here was done using the beam natural energy spread. This results in appreciably smaller tuneshifts (particularly for the smaller ≤ 6 Km rings and dogbone lattices with coupling bumps) when compared with a calculation done with vanishing energy spread.

Finally, we should recall that space-charge force is highly nonlinear and emphasize that the values quoted here describe the actual tuneshift only for particles with very small amplitude of betatron and synchrotron oscillations. Indeed most particles experience a sensibly smaller tuneshift: for example for MCH/65MV a particle launched with coordinates at "one-sigma" in all space coordinates *i.e.* $x = \sigma_x$, $y = \sigma_y$, $z = \sigma_z$, shows a FFT spectrum of the y-motion peaked at $\Delta\nu_y = -0.1$ *vs.* $\Delta\nu_y = -0.176$ for a particle with small amplitude of oscillations. (In a 3D gaussian density 68% of particles fall outside the 'one-sigma' region).

2.4 Results from tracking

As a first check of the MLI runs we verified reproducibility the linear optics for the various lattices as determined by MAD [12]. For the entries of the one-turn transfer matrix we generally found agreement through at least three or four digits.

The coding of the space-charge routines was checked against linear-theory by performing FFT [13] of particle orbits very close the beam centroid. Again, we found excellent agreement.

In Fig. 2 through 8 we show the results of tune-space exploration. In all cases the calculation was done by tracking a distribution of 200 particles for 150 turns (400 for the OCS lattice in Fig. 7) and monitoring the horizontal and vertical (*i.e.* mode I and mode II) rms eigen-emittances ε_I and ε_{II}. These eigen-emittances were calculated using the sigma matrix $\boldsymbol{\Sigma}$ obtained from the second moments of the tracked particle distribution at the end of each turn. Specifically, they were identified as the (absolute value of) the eigenvalues [9] of the matrix product $\boldsymbol{\Sigma J}$, ($\boldsymbol{J}$ is the 6×6 fundamental symplectic matrix).

We report color-density plots specifying for each working point the maximum value of the eigen-emittance achieved by the beam particles within the duration of tracking. The tunes specifying each working point are relative to the unperturbed (*e.g.* vanishing space charge) lattices. The black dots in the pictures locate the design working points.

The detuning of the lattices was done by inserting pure phase rotations at the end of the one-turn lattice or superperiods thereof, with proper matching so as not to perturb the value of the lattice functions. This amounts to a linear kick causing a discontinuity both in the particle transverse position and momentum.

The first set of figures (Fig.2) is relative to the MCH lattice with 65 MV total RF voltage, without ($N = 0$) and with space charge. We show results at the design current ($N = 2 \times 10^{10}$ par./bunch) and twice that value.

Not surprisingly, the growth in horizontal eigen-emittance turns out to be unaffected by the presence of space charge and here we only report the corresponding tune scan for the $N = 0$ case. In the region we explored, we found no horizontal emittance growth outside two well defined synchro-betatron resonances at $\nu_x + 2\nu_s = n$ and $\nu_x + \nu_s = n$.

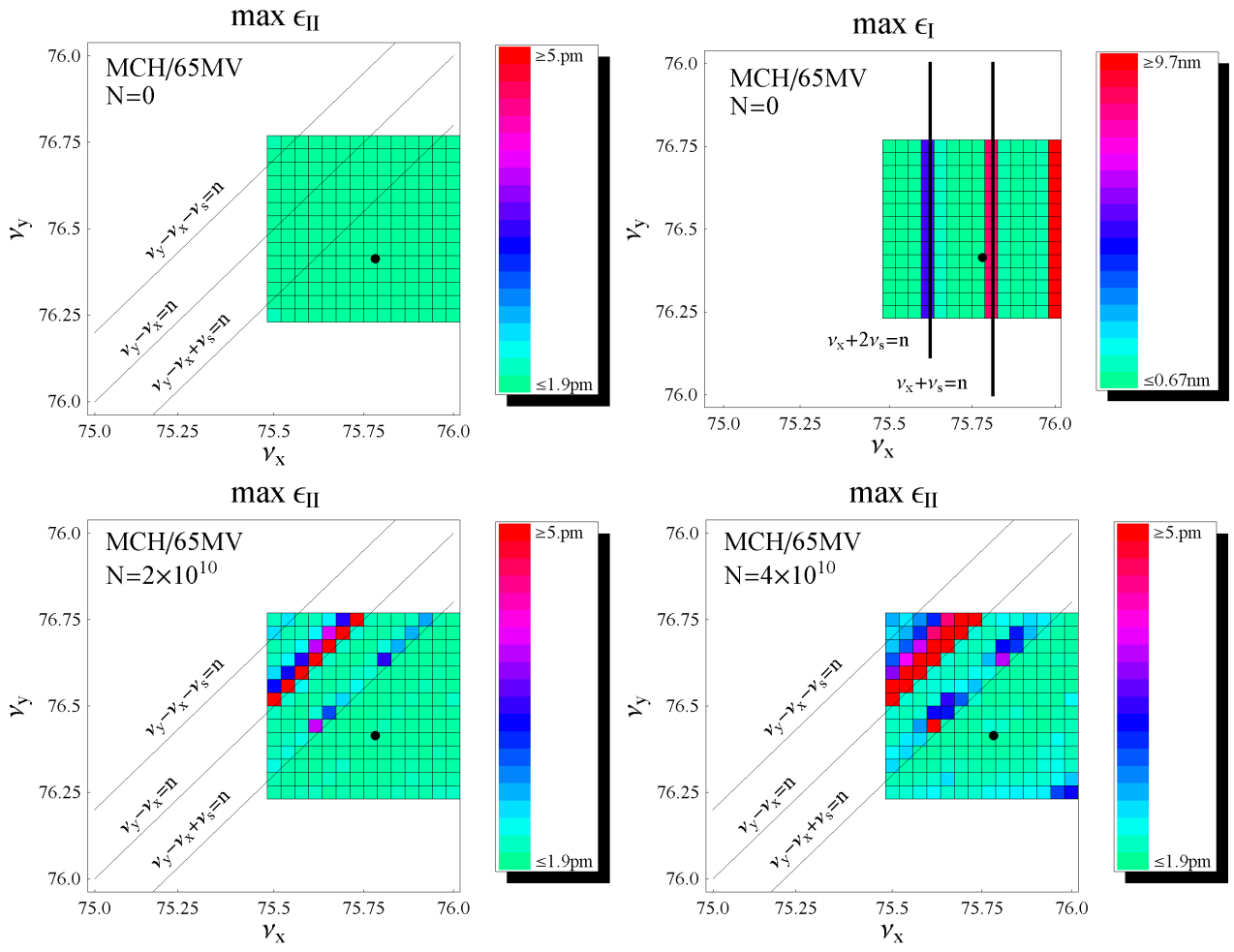

Figure 2: Tune scans for the MCH/65MV error-free lattice.

Vertically there is no apparent growth in the absence of space-charge, whereas some growth is apparent at $N = 2 \times 10^{10}$ and $N = 4 \times 10^{10}$ along difference coupling resonances and their synchotron-tune satellites. The form of the main resonance, $2\nu_y - 2\nu_x = 2n$ (this lattice has super-periodicity 2 and therefore only even $2n$ harmonics are allowed), suggests that this is a fourth-order resonance induced by the space-charge nonlinearities, *i.e.* a term x^2y in the equation of motion for vertical oscillations coming for a Taylor expansion of Eq. 2.

Indeed, one can construct a first-order simple dynamical model and verify that the strength of this term integrated over the lattice would be sufficient to cause a significant growth within a few turns. Notice that, as expected, the width of the resonance lies above the $\nu_y = \nu_x + n$ line because the tune depression causes particles to meet the resonant condition when the bare tune $\nu_y > \nu_x + n$. The width of the resonance is a measure of the tuneshift and is clearly larger for $N = 4 \times 10^{10}$ than $N = 2 \times 10^{10}$ (compare the two bottom pictures of Fig.2). The satellite resonances $2\nu_y - 2\nu_x \pm 2m\nu_s = 2n$ observed at $\pm 2\nu_s$ above and below the coupling resonance (only the $m = \pm 1$ resonances are clearly noticeable) are caused by the modulation of the space charge force resulting from synchrotron oscillations. This modulation occurs with a $2\nu_s$ frequency as the longitudinal charge density $\propto \exp(-z^2/2\sigma_z^2)$ depends quadratically on the longitudinal displacement z.

In the presence of lattice errors, one may expect further degradation of vertical emittance. In particular, lowest-order errors that favor coupling with the horizontal motion have the potential to cause the most damage. In this study we considered the impact of randomly distributed skew-quad like errors that may result, for example, from vertical offsets of the chromatic sextupoles. Specifically we considered a zero-average gaussian distribution of the offsets with a variance σ_{sxt} comparable to the one that would be required to generate a $\varepsilon_{II} = 2$ pm vertical eigen-emittance if radiation effects were included. For the MCH lattice such a value is $\sigma_{sxt} = 60$ μm (see [3]).

Already without space charge these errors excite detrimental resonances. In addition to the worsening of the difference resonances, some synchro-betatron resonances also appear. Presence of space charge makes things worse in two ways: they broaden the resonance width because of detuning and they favor decoherence of the large-amplitude emittance oscillations excited by the lattice resonances. The net effect can be observed in the left top picture of Fig 3 where in addition to the difference resonance lines already encountered in Fig 2 we observe sizeable emittance growth at $\nu_y = \nu_s + n$ and $\nu_y = 2\nu_s + n$.

In the left bottom picture of Fig 3 the presence of resonances is highlighted by a 1D scan of the tune plane where we vary the vertical tune as we keep the horizontal tune fixed to its design value ($\nu_x = 75.783$). The two curves represent the eigen-emittance maximum achieved within 150 turns without space charge (red curve) and with $N = 2 \times 10^{10}$ part./bunch (blue curve). We should remark that the strong integer resonance at $\nu_y = 76$ and the second-order resonance $2\nu_y = \nu_s + 76$ are already present in an error-free lattice without space charge.

The picture to the bottom right of Fig 3 shows the time evolution of the eigen-emittance for two seeds used in the random generation of the lattice errors. For comparison, the result for a run with no space charge (but with random lattice errors) is also reported (blue curve). The working point $\nu_y = 76.413$ is $\nu_y - 2\nu_s - 76 = 0.037$ away from the $2\nu_s$-resonance. In the absence of space charge this is sufficiently far away that there is no impact on the emittance, but not so when space charge is included.

The use of coupling bumps at each end of the long straight sections in the dogbone lattices was proposed as a way to tame the effect of space charge [10]. The coupling bumps consisting of a triplet of skew quadrupoles reduce the tuneshift by enlarging the vertical beam size. Linear theory (see Table 1) shows that they may be quite effective at achieving this goal. Unfortunately, they also appear to excite a number of resonances that reduce somewhat the

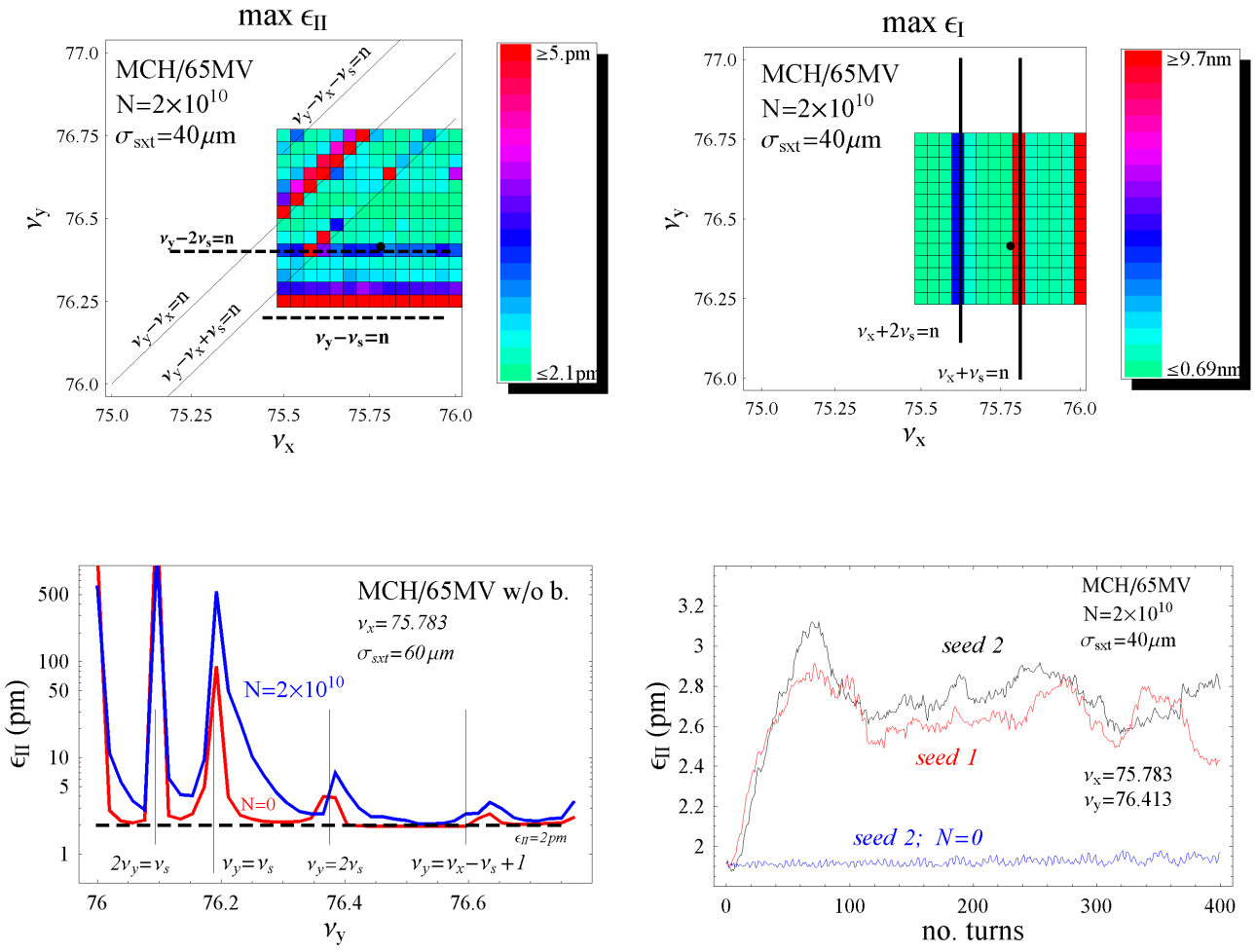

Figure 3: Tune scans for the MCH/65MV lattice with random vertical offset of sextupoles. In the left bottom picture: one dimensional ν_y tune-scan for given ν_x. Tracking with (blue line) is compared to tracking without space charge. Right bottom picture: evolution of vertical eigen-emittance at the design working point for two different seeds of random error distribution and for no errors (blue curve).

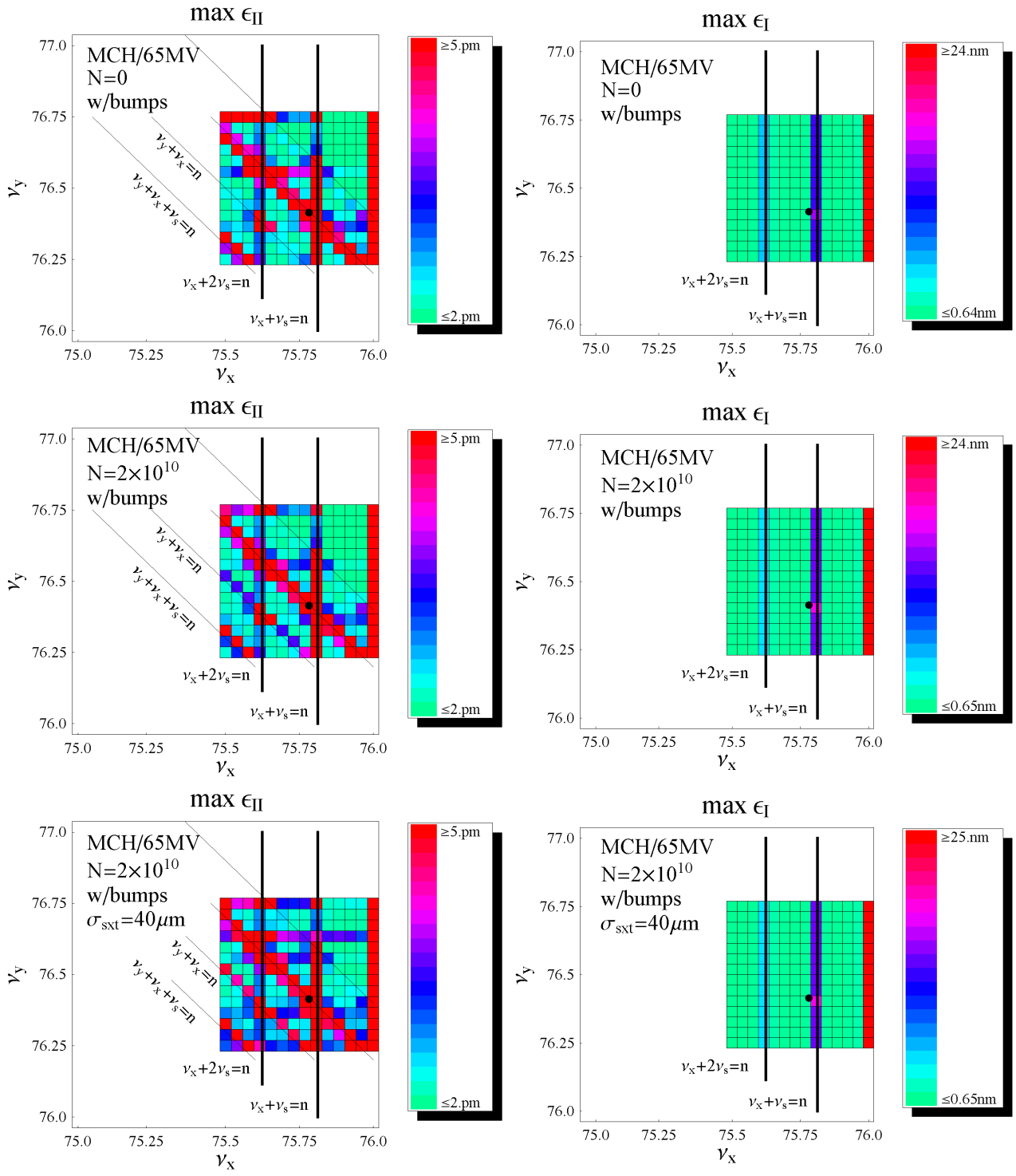

Figure 4: Tune scan for the MCH/65MV lattice with coupling bumps. From top to bottom: with and without space charge for ideal lattice and with space charge with lattice errors).

usable regions of the tune-space, see Fig. 4. One effect is to pass onto the vertical emittance some growth at resonances that without coupling bumps only affect the horizontal emittance. But there are also some additional (sum) resonances that were previously absent. All these resonances are manifest already before adding space charge. In fact, from these pictures the only visible effect of space charge is in the additional excitation of the sum resonance $\nu_x + \nu_y = n$, (left picture in the middle row of Fig. 4).

There are patches of tune space unaffected by resonances and which, presumably, could accommodate bunches with a number of particles larger than $N = 2 \times 10^{10}$. However, these patches are further reduced when a distribution of random skew-quadrupoles is superposed to the ideal lattices (left bottom picture in Fig. 4) and they do not enclose the currently proposed working point.

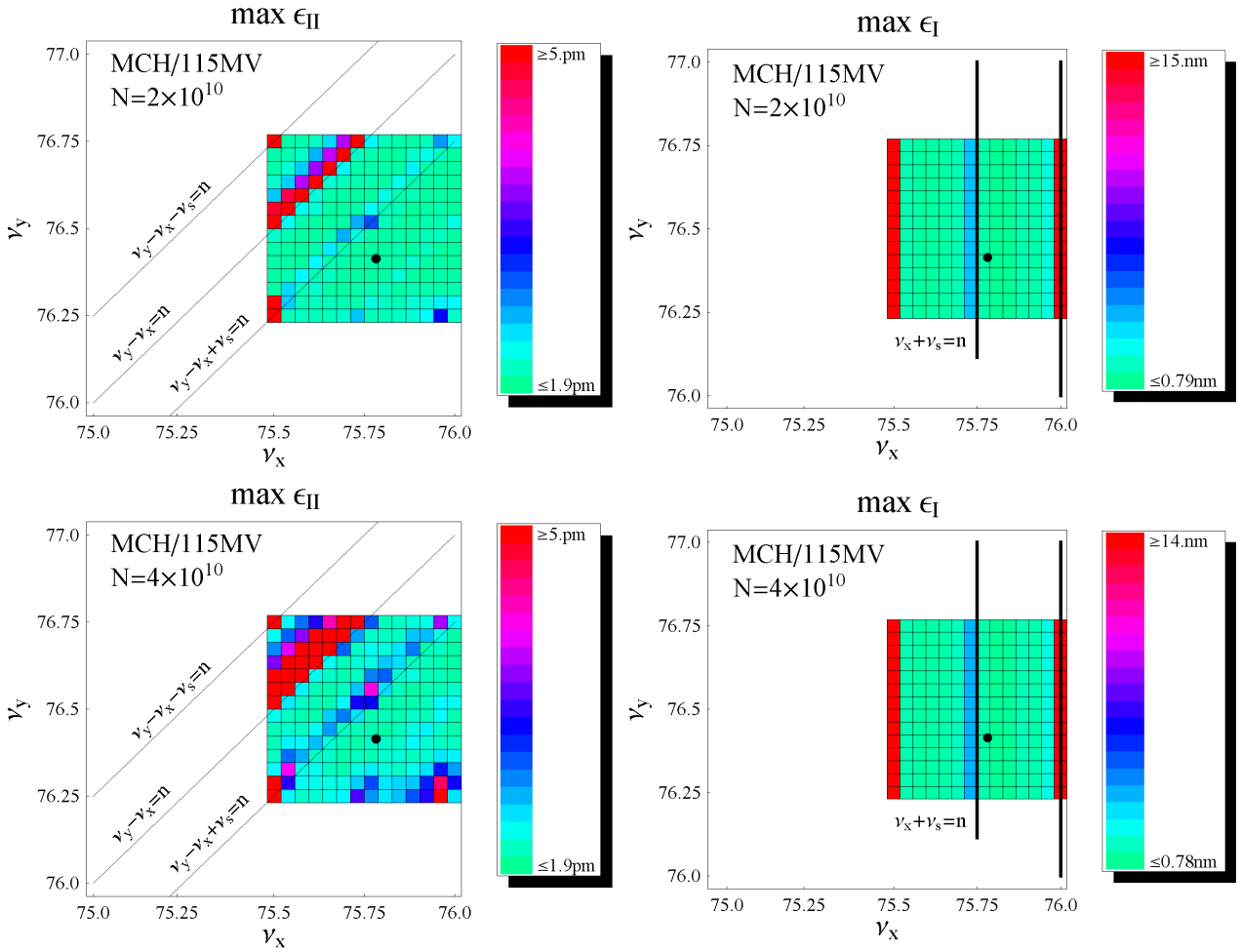

Figure 5: Tune scan for the MCH/115MV lattice.

Not surprisingly, a larger RF voltage (see Fig. 5) shows the same patterns of vertical emittance growth as for the MCH/65MV lattice. The synchotron-betatron resonances are

shifted in accordance to a larger synchrotron tune ($\nu_s = 0.25$ *vs.* $\nu_s = 0.19$ in the 65MV case) and their effect slightly enhanced because of the large longitudinal beam density resulting from a smaller bunch length.

The tune-scan results for the TESLA damping ring are summarized in Fig. 6. Again, in the absence of space charge (not shown) there is no noticeable emittance growth whereas some growth is apparent with space charge. In the absence of lattice errors (left top picture) the growth takes place along difference resonances. Compared with the MCH case the width of these resonances appears thicker partly because of the proximity of the satellite resonances $\nu_y - \nu_x \pm \nu_s = n/2$ as the synchrotron tune is now smaller ($\nu_s = 0.075$). Also, the difference resonance lines are more closely spaced as the TESLA lattice does not share the super-periodicity 2 of the MCH lattice. This is the 'C-shaped' lattice contained in the original TESLA TDR proposal. An 'S-shaped' variant to this lattice exhibiting a higher degree of symmetry is considered in Sec. 3 (SAD simulations) and indeed it displays better beam dynamical properties.

The tune-scan in the presence of lattice errors is dominated by the strong $\nu_y = \nu_s + n$ resonance. The random vertical displacement of the sextupoles here had a variance $\sigma_{sxt} =$ 6 μm, close to the 8 μm value that would be responsible for the 2 pm vertical emittance in the presence of radiation [3].

In the bottom left picture of Fig. 6 we show the result of a calculation done with a realistic wiggler model based on a scaled-down version of the CESR-c superconducting wigglers. By contrast, in all other calculations shown in this report the wigglers were modelled using standard lattice 'linear' elements (combined function dipoles, drifts). Comparison with the top left shows virtually no difference, and would seem to indicate little impact from the wiggler nonlinearities.

The final set of tune-scans reported is relative to the smaller circumference (6 Km) OCS lattice. From the linear theory tuneshift one already expects a smaller impact by space charge: indeed Fig. 7 shows no apparent effect. The tuneshift, however, is not completely negligible; for instance, it is larger than in the dogbones with coupling bumps where some space charge effect was still noticeable. It is likely that the good behavior of the OCS lattice may be due, in part, to its high degree of symmetry. Inclusion of lattice errors shows some impact on emittance growth Fig. 8 but most of the tune-space region explored remains clear.

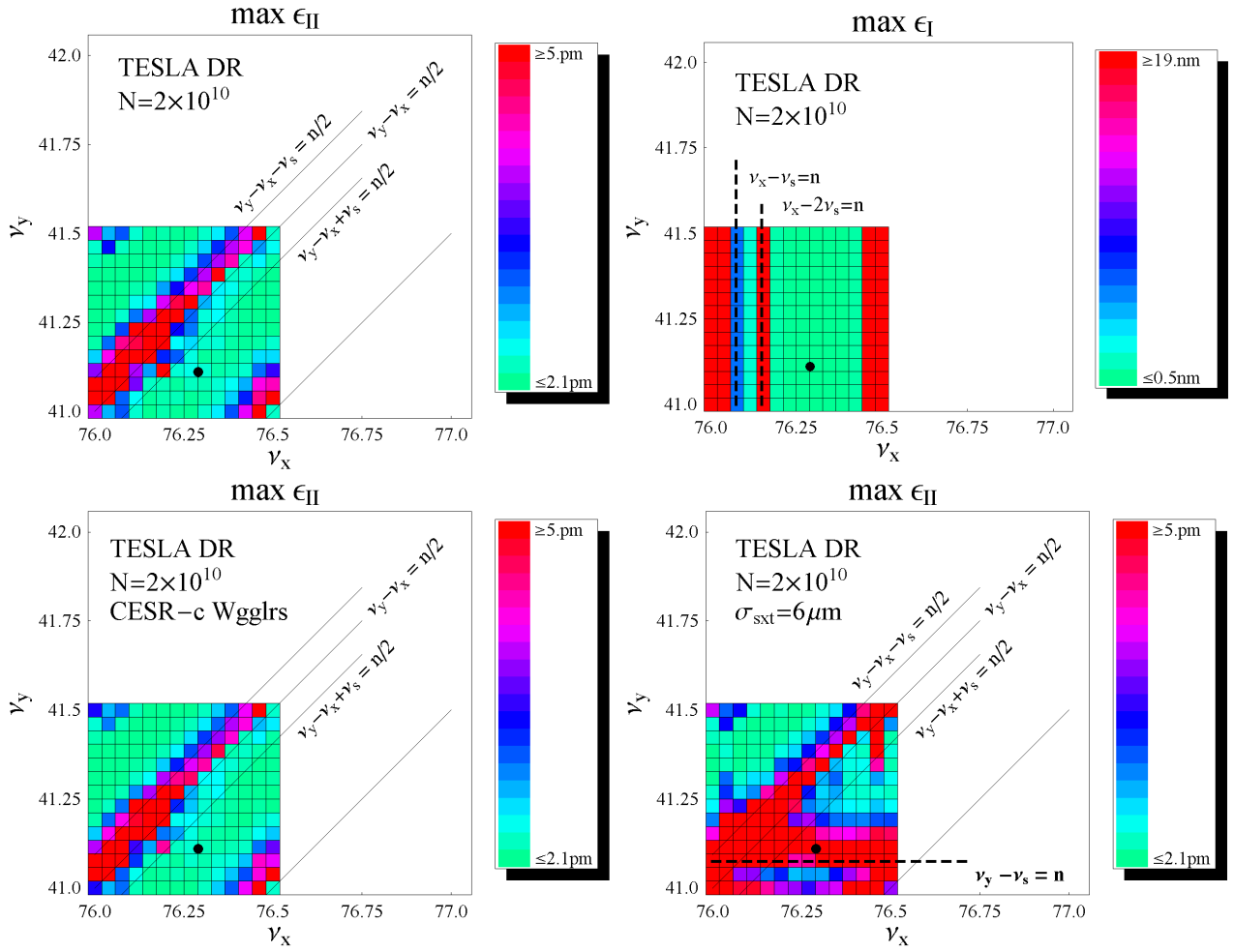

Figure 6: Tune scan for the TESLA DR (This is the C-shaped lattice of the original TESLA TDR proposal). In the bottom figures the scaled-down CESR-c wiggler model was used (left) and a random vertical offset of sextupoles was added (right).

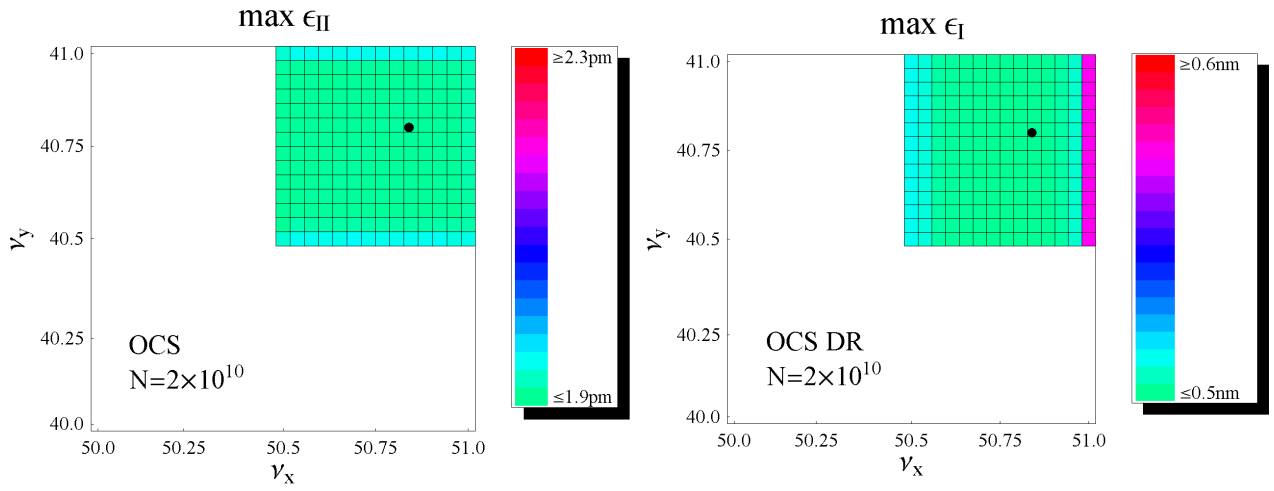

Figure 7: Tune scans for the OCS.

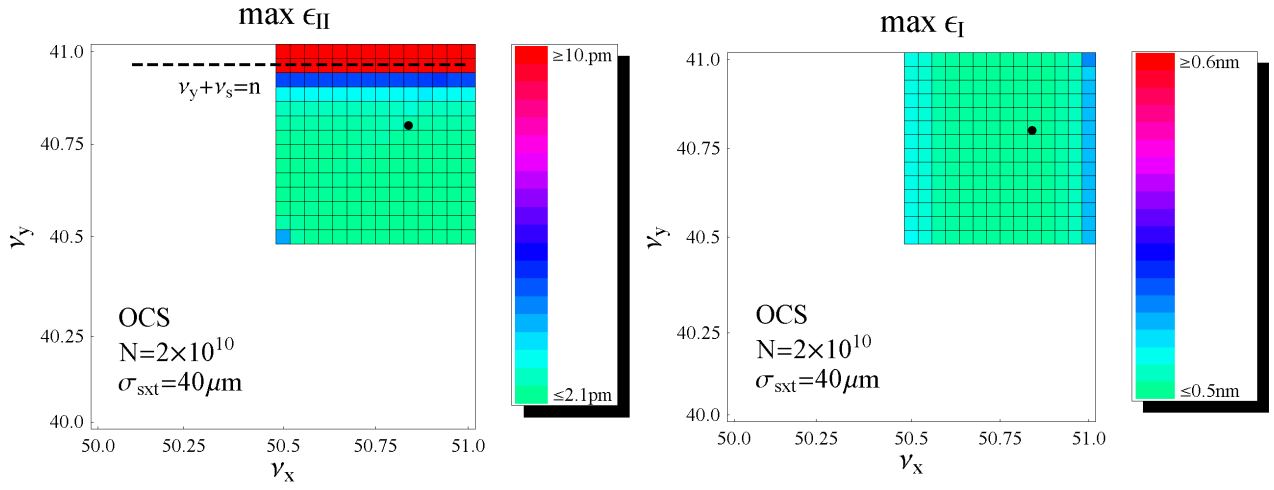

Figure 8: Tune scans for the OCS with random vertical offset of sextupoles.

3 Space charge study using SAD

3.1 Beam Envelope with Space Charge

Estimation of space charge force requires calculation of the beam envelope along the beamline. As the beam envelope is also affected by the space charge, SAD performs iterative calculation until convergence. The equilibrium beam envelope $\langle X_i X_j \rangle$, a 6 by 6 matrix, is the matrix of second-order moments around the beam center. At the entrance of the ring it must satisfy the equilibrium condition [14]

$$\langle X_i X_j \rangle = M \langle X_i X_j \rangle M^T + r_{ij} \ , \tag{14}$$

where M is the 6D linear transfer matrix around the ring, and r_{ij} is a matrix representing excitation matrix by synchrotron radiation. The matrix M consists of a symplectic part representing the lattice (with space charge defocusing) and a non-symplectic part representing radiation damping.

Space charge nonlinearities will be included in particle tracking, but for the envelope calculation in Eq. (14), only the linear part of the space charge force evaluated at beam center is used. The space charge force is applied at the entrance of each element as a thin lens. For drift elements, which can be much longer than magnetic elements, accuracy is improved by additionally applying the space-charge force in the center.

The equilibrium emittances are obtained as the eigenvalues of the beam envelope and are denoted as $\varepsilon_I, \varepsilon_{II}, \varepsilon_{III}$. In the limit of vanishing coupling I, II, and III correspond to the x, y, and z planes. For planar machines such as the ILC Damping Rings, the mode-II (=nearly vertical) emittance, ε_{II}, becomes very small. To obtain a realistic value of ε_{II}, one method is to add machine errors to some components in the ring; for example one can add vertical offsets to the sextupoles. The envelope method can then be used to calculate the effect of space charge on the equilibrium emittance. Figure 9 shows the vertical emittance resulting from random vertical misalignement of the sextupoles in the TESLA damping ring, with and without space charge. In this case, space charge increases the equilibrium vertical emittance by approximately 50%.

As an alternative to misaligning the sextupoles, one can generate vertical emittance by giving an artificial value to the envelope at the entrance of the ring. This is equivalent to an artificial radiation excitation r_{ij}. The resulting beam envelope still matches the beam optics around the ring, except for mode II, but the mismatch is small unless radiation damping is very large. Using random sextupole misalignments to generate vertical emittance has the drawback that the vertical emittance depends on the seed of the random errors, so for the studies described here the vertical emittance was generated by using an artificially excited beam envelope.

3.2 Calculation of the Space Charge Force

Particle tracking with space charge in SAD makes use of the envelopes as determined by the method discussed in the previous section. A weak-strong model is used, with a Gaussian

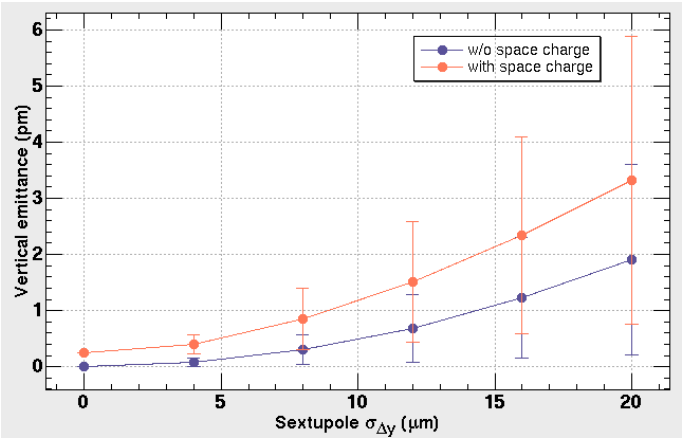

Figure 9: Equilibrium mode-II emittance with(orange)/without(blue) space charge as functions of the vertical random offset of the sextupoles in the TESLA damping ring with the coupling bump. 12 random number seeds are used for each r.m.s. offset $\sigma_{\Delta y}$. The space charge enhances the mode-II emittance by about 50%. The emittance for $\sigma_{\Delta y} = 0$ is nonzero with space charge, as the coupling bump no longer closes due to the space charge. The particles per bunch is $N = 2 \times 10^{10}$.

distribution for the 'strong' beam. As the beam is highly ultra-relativistic, only the component of the space-charge force perpendicular to the beam axis is relevant. Under these assumptions the space-charge potential reads

$$U(x, y, z) = f(\xi, \eta) \exp\left(-\frac{z^2}{2\sigma_z^2}\right) \ , \tag{15}$$

where f, the 2D electrostatic potential in the transverse plane, is a function of ξ/σ_ξ, η/σ_η, and the aspect ratio $R = \sigma_\eta/\sigma_\xi$, where ξ and η are the major and the minor axes of the transverse beam ellipse, respectively.

To reduce computation time, SAD first calculates $f(\xi, \eta)$ at $60\times60\times20$ mesh points within the range $0 \le \xi/\sigma_\xi \le 15$, $0 \le \xi/\sigma_\eta \le 15$, $10^{-5} \le R \le 1$ using semi-analytical numerical integration. The mesh points are equally separated in the (ξ, η) plane, and logarithmically separated in the R-direction. During tracking, the force is obtained from values on the mesh points using cubic splines interpolation. As the cubic spline is continuous up to the second-order derivatives, the force satisfies the symplectic condition within machine precision. If a particle falls outside the mesh region, the original semi-analytic formulae is applied. This interpolation technique is highly efficient: as a result, the time employed by the code to compute space charge forces is only a fraction of the overall CPU time.

SAD tracks particles in the full 6D phase space with full account of nonlinearities (*e.g.* in a drift element the nonlinearities generated by the square root of the momentum part of the Hamiltonian), magnet fringe-fields effects, etc. Inclusion of synchrotron radiation during tracking is an option but this option was not used in the calculations discussed in this paper.

3.3 Diffusion due to Space Charge

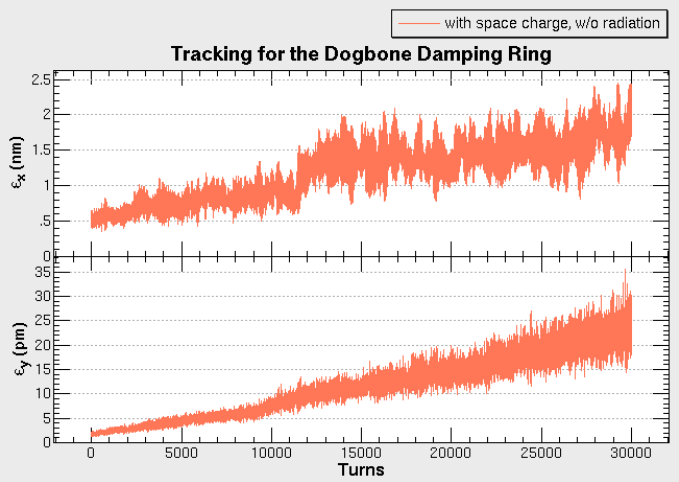

Figure 10: The emittance growth observed by the tracking simulation with space charge for the TESLA damping ring with the coupling bump. Both the mode-I (upper) and the mode-II (lower) emittances grow roughly linear in the number of turns. The synchrotron radiation is turned off in the tracking. The number of tracked particles is 100. The particles per bunch is $N = 2 \times 10^{10}$.

A typical phenomenon encountered in our tracking simulations is a diffusion-like emittance growth in phase space. Figure 10 shows such an example of diffusion of mode-I and mode-II emittances. As shown in this figure, both mode-I and mode-II emittances show nearly linear growth of the emittance, justifying the use of the term "diffusion". In the presence of such a linear growth, the equilibrium emittance can be estimated by

$$\varepsilon = \varepsilon_0 + \frac{n_d}{2}\left(\frac{\Delta\varepsilon}{\Delta n}\right) \ , \tag{16}$$

where ε_0 is the equilibrium emittance without the space charge and n_d the number of turns corresponding to the radiation damping time. Since tracking with synchrotron radiation is time consuming (indeed much more time consuming than calculating space charge), we use Eq. (16) to estimate the equilibrium emittance while performing tune scans to study the dependence of the emittance growth on the working point in the tune-space. No emittance growth is observed in the absence of space charge.

In the simulations we kept the 'strong' beam unchanged. One could update the strong beam during tracking to account for the growth of the transverse envelopes in the 'weak' beam diluting the strength of the space charge force. By not doing so we overestimate the effect of space charge on emittance growth.

The number of particles used for tracking was typically 100. We verified that the results did not change significantly by increasing the number of tracked particles to 400.

3.4 Tune Scans

The tune scans were performed for various damping-ring reference lattices without lattice errors. In each case, changes in tune were achieved by inserting quadrupoles into the lattice and varying their strengths, while matching the appropriate optical functions. The equilibrium emittances were obtained from Eq. (16), with the linear growth rate ($\Delta\varepsilon/\Delta n$) calculated by tracking up to 400 turns without radiation.

Figures 11 show the results for the TESLA 'S-shaped' damping ring lattice. Note that the coupling bumps were adjusted to produce a properly round beam in the straights.

The MCH lattice was studied with two different RF voltages, 54 MV and 115 MV, corresponding to bunch lengths of (approximately) 10 mm and 7 mm; the results are shown in Figures 12 and 13

In general, although there are areas associated with resonance lines where significant emittance growths are observed, there are also substantial areas of tune space where there is minimal emittance growth. The coupling bumps do not necessarily improve the situation, and can themselves drive new resonances (*e.g.* resonance lines like $\nu_x + \nu_y \pm \nu_z = 2N$) or make exiting ones stronger (*e.g.* $2\nu_y \pm \nu_z = 2N$). This may be more serious for the MCH lattice with 115 MV RF, which has a larger synchrotron tune than the other lattices, reducing the "safe areas". Also the MCH lattice shows stronger horizontal resonances than the "S-shaped" TESLA lattice, with or without coupling bumps.

Results for the 6 km lattices are shown in Figures 14. The OCS looks the safest of all the reference lattices from the point of view of space charge; however, the BRU lattice looks worse even than the dogbone lattices. Note that the energy of the BRU lattice, 3.74 GeV is somewhat lower than the other lattices, which are all around 5 GeV.

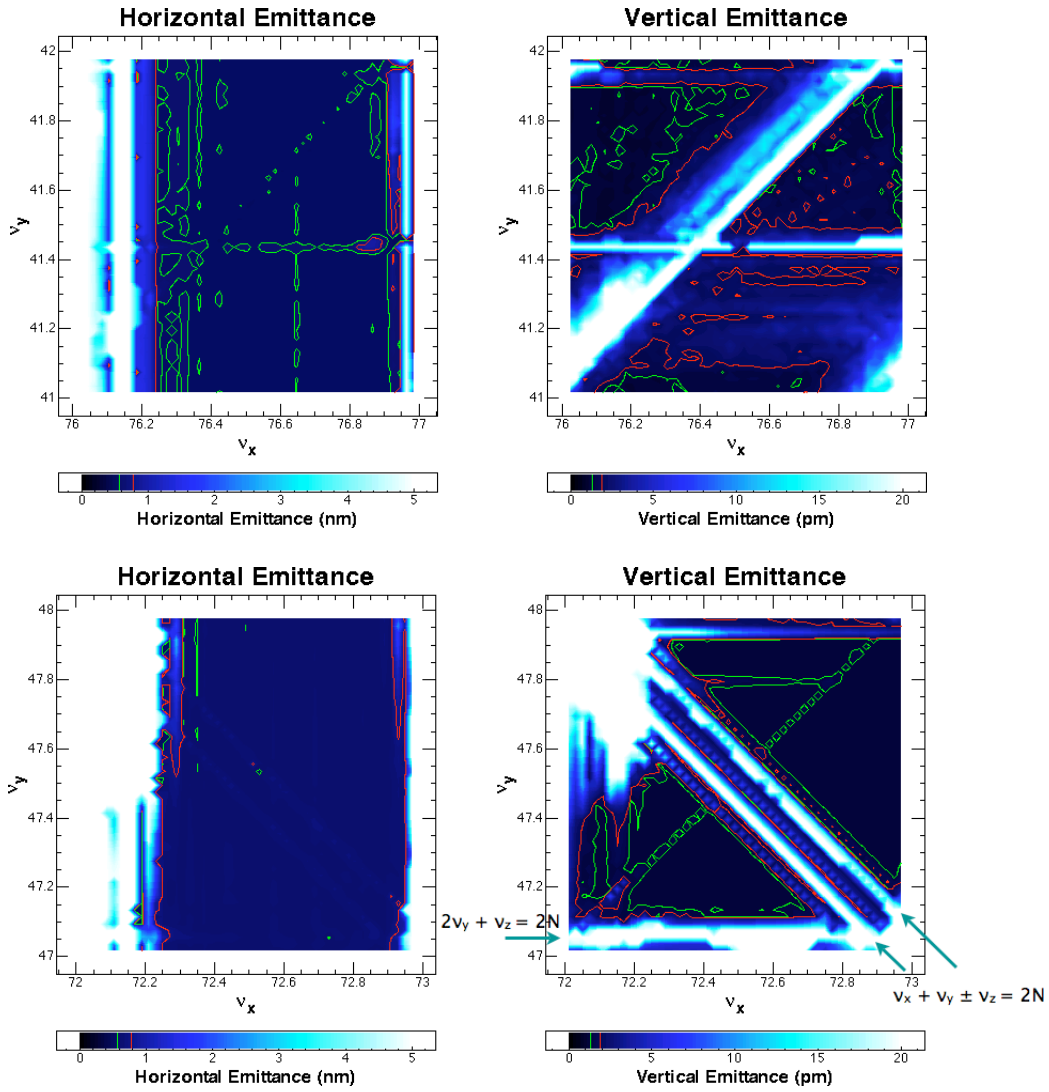

Figure 11: The tune scan of the emittance growth observed by the tracking simulation with space charge for the 'S-shaped' TESLA DR lattice without (upper) and with (lower) the coupling bump. The left ones show the Mode-I (nearly horizontal) emittance and the right ones Mode-II (nearly vertical). The particles per bunch is $N = 2 \times 10^{10}$. The number of tracked particles is 100.

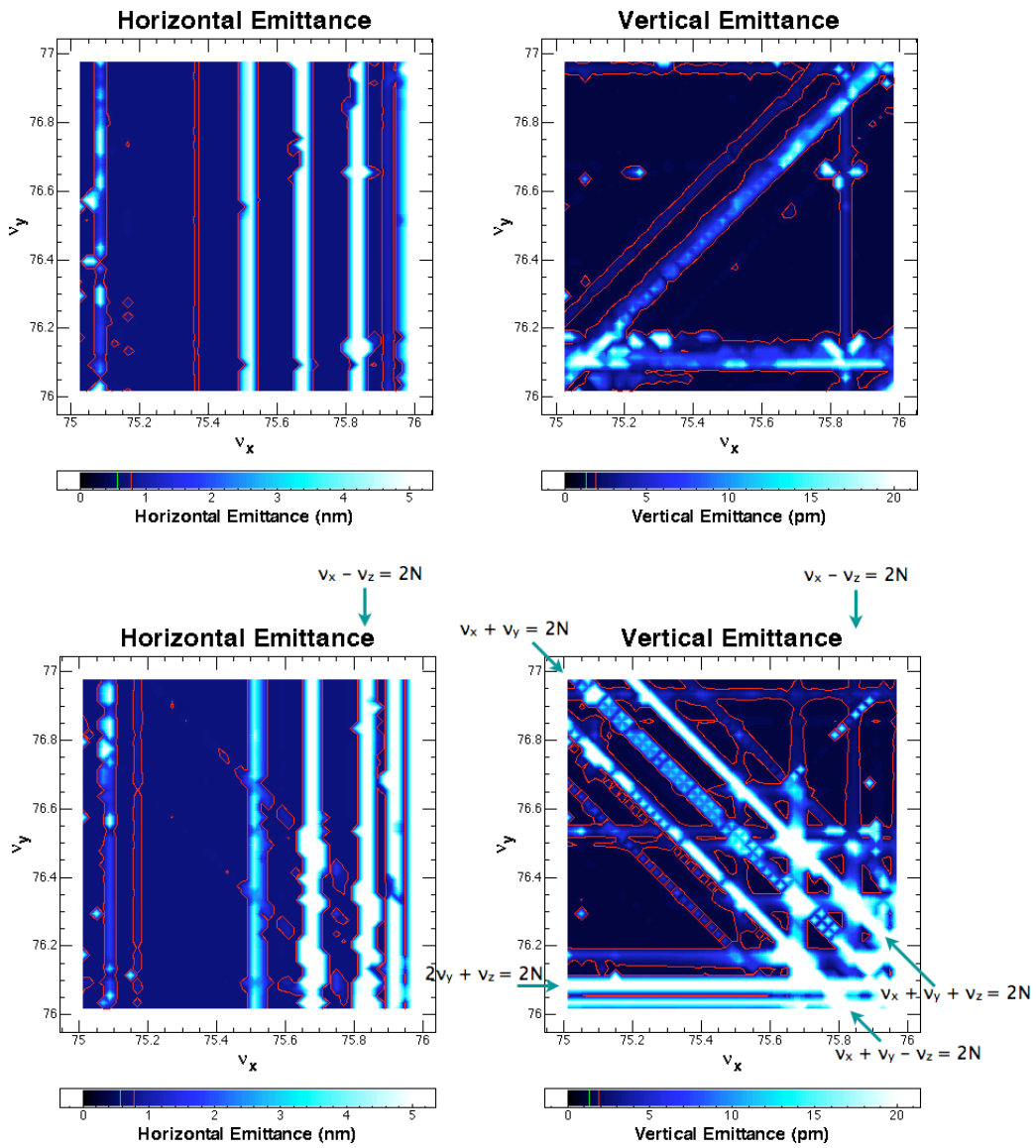

Figure 12: The tune scan of the emittance growth observed by the tracking simulation with space charge for the MCH/54MV lattice without (upper) and with (lower) the coupling bump. The rf voltage is 54 MV. The left ones show the Mode-I (nearly horizontal) emittance and the right ones Mode-II (nearly vertical). The particles per bunch is $N = 2 \times 10^{10}$. The number of tracked particles is 100.

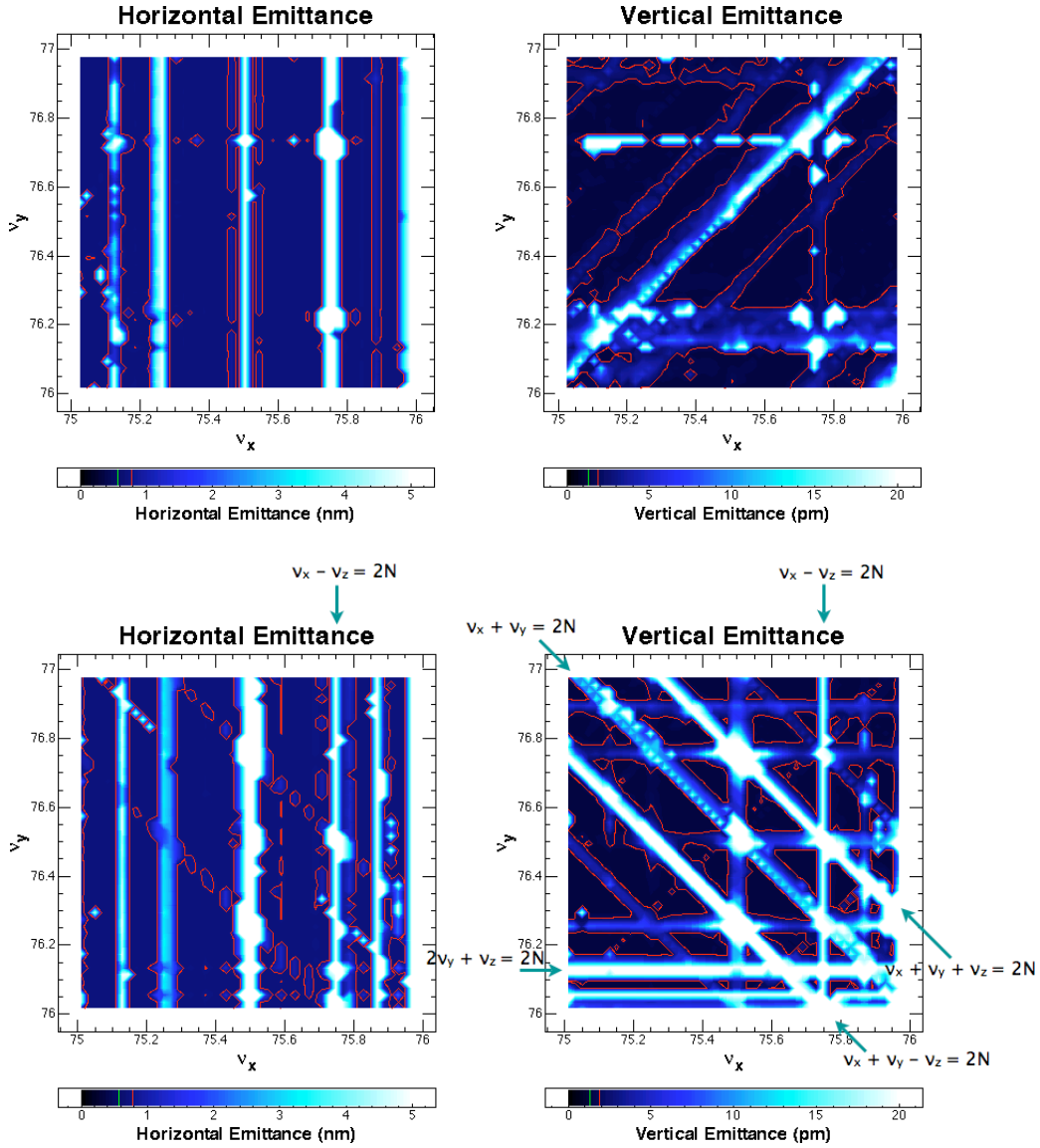

Figure 13: The tune scan of the emittance growth observed by the tracking simulation with space charge for the MCH/115MV lattice without (upper) and with (lower) the coupling bump. The left ones show the Mode-I (nearly horizontal) emittance and the right ones Mode-II (nearly vertical). The rf voltage is 115 MV, which makes the sum resonance sidebands $\nu_x + \nu_y \pm \nu_z = 2N$ farther from $\nu_x + \nu_y = 2N$ line, reducing the safe area in the case with the coupling bump. The particles per bunch is $N = 2 \times 10^{10}$. The number of tracked particles is 100.

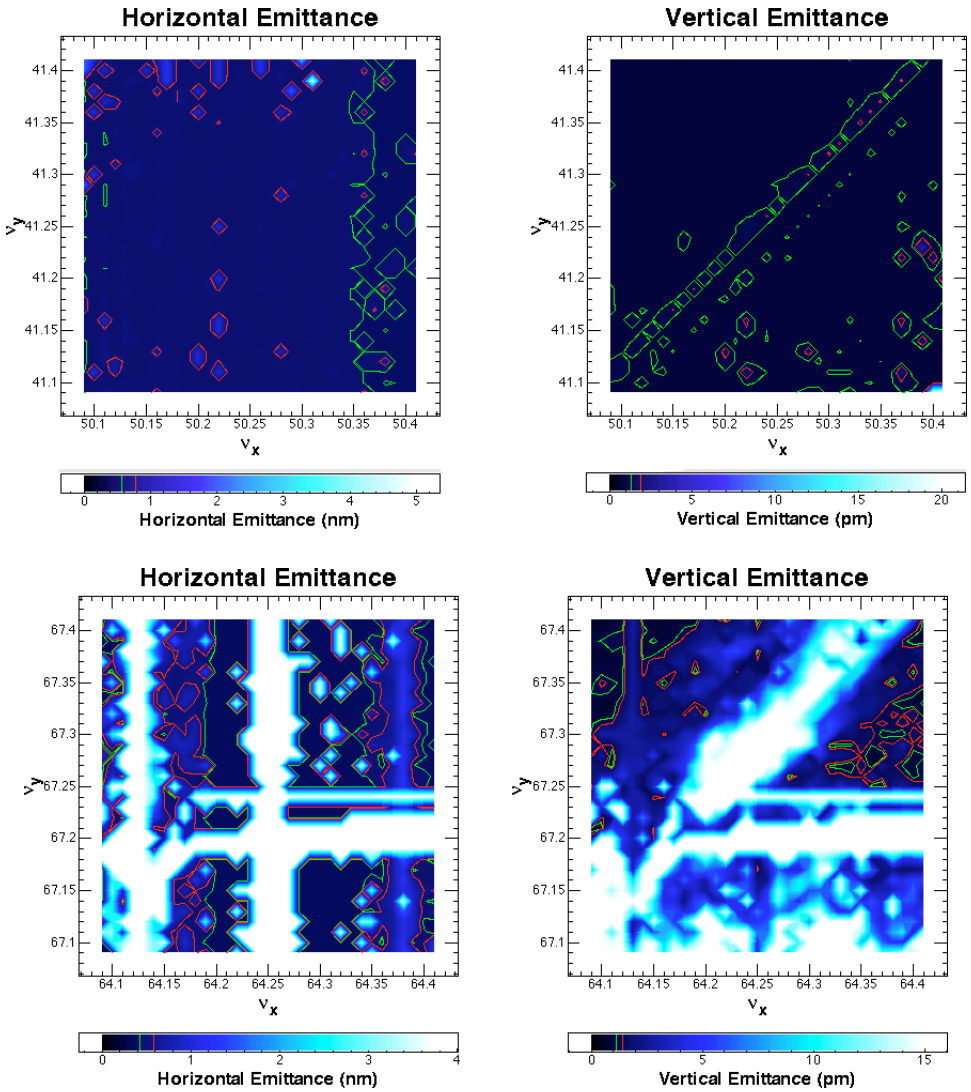

Figure 14: The tune scan of the emittance growth observed by the tracking simulation with space charge for the 6 km rings, OCS (upper) and BRU (lower). The left ones show the Mode-I (nearly horizontal) emittance and the right ones Mode-II (nearly vertical). Note that the scanned tune spaces are smaller than the previous figures. BRU's energy is 3.74 GeV. The particles per bunch is $N = 2 \times 10^{10}$. The number of tracked particles is 100. Notice that the region of tune space explored here is smaller than in the previous figures.

4 Conclusions

A summary of our conclusions is the following:

- The 6 Km OCS lattice stands out as the safest choice among the lattice considered. The shorter circumference is a factor accounting for the mild impact of space charge compared to the dogbone lattices, but apparently not the only one. The BRU lattice has similar circumference (and somewhat lower energy) but behaves poorly. The high degree of symmetry of the OCS lattice does seem to play a decisive role in mitigating harmful resonances.

- The 16-17 Km dogbone lattices are clearly more vulnerable to space charge and at higher risk, but, on paper, they may not be impossible to operate. There are patches of tune space far enough from dangerous resonances whether or not errors are included. The presence of these resonances, however, limits the flexibility in the choice of the working point and may induce conflict with other requirements.

- As a qualification of the previous point, we should add that some dogbone lattices are preferable to others: for example the "C-shaped" TESLA DR, mostly because of poor symmetry, is not very good. The "S-shaped" version of the TESLA DR is clearly superior.

- The MCH lattice has a large synchrotron tune that causes resonance lines to be more dispersed in tune space. This may be more limiting to the choice of the working point.

- In general, it appears that the coupling bumps do not offer a decisive advantage: as they come at the price of exciting some other resonances. Their effectiveness depends somewhat on the lattice.

- For the "S-shaped" TESLA DR the coupling bumps can restore some flexibility in the choice of the working point as the locations of dangerous resonances with and without bumps are quite different. One can argue that in this case coupling bumps overall make a larger area of tunespace accessible.

- For MCH it is not obvious that the coupling bumps are generally helpful as the web of the excited resonances is more widely spread than w/o bumps. Still, if the MCH lattice is to be chosen we may recommend that coupling bumps be installed to give some additional flexibility.

- We have not carried out a detailed study of the smaller (3km) lattices, though we expect that space charge should not be an issue for these configurations.

5 Acknowledgements

We gratefully acknowledge K. Ohmi, Y. Ohnishi, and A. Wolski, for assistance and useful discussions, and H. Koiso for translation of the MAD input decks to SAD. Work supported in part by Department of Energy contract DE-AC02-05CH11231.

References

[1] SAD Home page at http://acc-physics.kek.jp/SAD

[2] A. Dragt, et al., MARYLIE Manual, University of Maryland, College Park, MD (2004).

[3] J. Gao, S. Guiducci, and A. Wolski Editors, Recommendations for the ILC Damping Rings Baseline Configuration, LBNL Report LBNL-59449, Berkeley (2006).

[4] M. Furman and A. Zholents, Comparisons of Beam-Beam Cose Simulations, CBP Tech Note-59, LBNL, Berkeley (1996).

[5] M.Bassetti and G.A. Erskine, CERN-ISR-TH/80-06, Cern Report, Geneva (1980).

[6] Q. Ji and M. Furman, private communication.

[7] S. Wolfram, The Mathematica Book 4th Ed., Wolfram Media/Cambridge University Press, 1999.

[8] TESLA Technical Design Report, `http://tesla.desy.de/new_pages/TDR_CD/start.html`

[9] A. Wolski, A Simple Way to Characterize Linear Coupling in a Storage Ring, LBNL Report, LBNL-54774, (2004).

[10] W. Decking and R. Brinkmann, Proc. 7th Eur. Part. Acc Conf. EPAC2000, p. 1024, M. Regler Ed. (2000).

[11] M. Venturini, First-Order Space-Charge Tuneshift in a Linearly Coupled Lattice, LBNL Report LBNL-57664, Berkeley (2005).

[12] H. Grote, The MAD Program, User Manual CERN Report CERN/SL/90-13 (A), Geneva (1996).

[13] R. Bartolini *et al.*, Tune Evaluation in Simulations and Experiments, CERN Report, CERN SL/95-84 (AP), Geneva (1995).

[14] K. Ohmi, K. Hirata, and K. Oide, Phys. Rev. E49,751 (1994).